THE JOURNAL OF PHYSICAL CHEMISTRY B

Article

pubs.acs.org/JPCB

Origin of Abrupt Rise in Deuteron NMR Longitudinal Relaxation Times of Protein Methyl Groups below 90 K

Liliya Vugmeyster,*[,†] Dmitry Ostrovsky,[‡] and Andrew S. Lipton[§]

[†]Department of Chemistry and [‡]Department of Mathematical Sciences, University of Alaska Anchorage, 3211 Providence Drive, Anchorage, Alaska 99508, United States

[§]Pacific Northwest National Laboratory, Richland, Washington 99354, United States

Supporting Information

ABSTRACT: In order to examine the origin of the abrupt change in the temperature dependence of ^{2}H NMR longitudinal relaxation times observed previously for methyl groups of L69 in the hydrophobic core of villin headpiece protein at around 90 K (Vugmeyster et al. *J. Am. Chem. Soc.* **2010**, *132*, 4038−4039), we extended the measurements to several other methyl groups in the hydrophobic core. We show that, for all methyl groups, relaxation times experience a dramatic jump several orders of magnitude around this temperature. Theoretical modeling supports the conclusion that the origin of the apparent transition in the relaxation times is due to the existence of the distribution of conformers distinguished by their activation energy for methyl three-site hops. It is also crucial to take into account the differential contribution of individual conformers into overall signal intensity. When a particular conformer approaches the regime at which its three-site hop rate constant is on the order of the quadrupolar coupling interaction constant, the intensity of the signal due to this conformer experiences a sharp drop, thus changing the balance of the contributions of different conformers into the overall signal. As a result, the observed apparent transition in the relaxation rates can be explained without the assumption of an underlying transition in the rate constants. This work in combination with earlier results also shows that the model based on the distribution of conformers explains the relaxation behavior in the entire temperature range between 300 and 70 K.

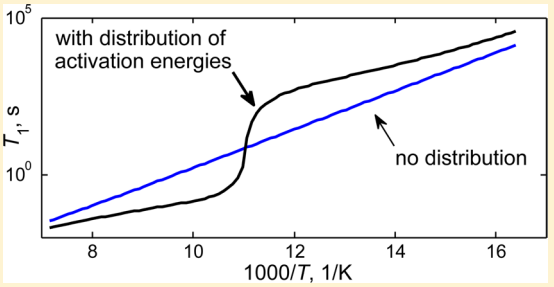

INTRODUCTION

Methyl groups are very important in the functioning of protein molecules and such events as protein folding, ligand binding, and intermolecular interactions.[1−10] NMR spectroscopy plays an important role in investigations of methyl's dynamics due to its ability to render site-specific resolution and techniques that cover a wide range of time scales of motions.[1,3,10−14] Deuteron nuclei are sensitive probes and, when incorporated into a protein, allow for detailed investigations of the dynamics.[2,5,7,9] Deuteron NMR relaxation rates are usually dominated by the interaction of the nuclear electric quadrupole moment with the electric field gradient at the site of the nucleus. The deuteron has a relatively small electric quadrupole moment, which makes it easy to work with experimentally.

For studies of methyl group dynamics, we chose a small model protein, chicken villin headpiece subdomain (HP36),[15] which has been extensively used in various protein folding and dynamics investigations.[15−28] The small size of this protein allows for a relatively easy preparation of samples with selectively deuterated methyl groups at desired positions, using solid-state peptide synthesis.

Our previous measurements pointed to an existence of an unexpected phenomenon when the temperature is lowered below 95 K.[28] Namely, we observed an abrupt increase of several orders of magnitude in the deuteron longitudinal relaxation times (T_1) for methyl groups of the L69 residue, located in the hydrophobic core of HP36. The main mechanism of the longitudinal relaxation is the three-site hops of the deuterons.[5] If there is a single rate constant governing this process, then, in the slow limit with respect to the Larmor frequency, the relaxation time is proportional to the inverse of the rate constant.[29] In this case, the abrupt increase in the NMR relaxation times should indicate freezing of methyl group dynamics.

The goal of this work is to investigate the nature of this effect more thoroughly. First, we confirm that this apparent transition in the relaxation times is present for several other methyl groups in the hydrophobic core, belonging to residues L61 and L75 (Figure SI1 in the Supporting Information). If one assumes that the relaxation is governed by a single three-site hop process, then the conclusion that there is an abrupt drop in the rate constant seems to be inevitable. However, recent relaxation data[30] on the same sites over a higher temperature range of 300−140 K suggest the presence of multiple conformers. We developed a model in which each conformer is distinguished by its unique value of activation energy barrier, which leads to a

Received: March 2, 2013
Revised: April 27, 2013
Published: April 29, 2013

distribution of three-site hop rate constants at each temperature. The samples used in these studies had single-site deuteron labels, so that the observed distribution reflects conformational heterogeneity of individual residues.

We will show below that this distribution explains the observed abrupt increase in the deuteron NMR relaxation times without invoking the assumption of the methyl group freezing transition. A key factor behind this phenomenon is a sharp drop of signal intensity for the conformers, for which the three-site hop rate constants are on the order of quadrupolar coupling constant.

The apparent transition in the dynamics has also been noted by many neutron diffraction studies, in which it is observed as an inflection point in the temperature dependence of the atomic mean square displacement.[31−33] The temperature of this inflection point, which corresponds to the onset of anharmonic modes, varied for different systems from 150 to 100 K. We discuss a connection between insights emerging from our studies with conclusions of the neutron diffraction investigations.

MATERIALS AND METHODS

Sample Preparation. FMOC-leucine-5,5,5-d_3 used for incorporation of selective deuteron labels was purchased from Cambridge Isotopes Laboratories (Andover, MA). The labeling pattern is in 1:1 ratio for each methyl group. All protein samples were synthesized commercially (Thermofisher Scientific, Inc.) by solid-state peptide synthesis with incorporation of the deuterated leucine at selected sites. Each of the samples had deuteron labels in methyl groups of only *one* of the leucine residues. The samples were purified by reverse-phase HPLC. The identity and purity of the samples were confirmed by both mass spectroscopy and reverse-phase HPLC. Lyophilized powders were dissolved in water and the pH was adjusted to about 6 using NaOH/HCl. HP36 is expected to be folded in this range. We have previously confirmed the refolding procedure for HP36 by measuring several chemical shift values, which agreed with the values reported for the folded protein in solution.[28] The sample hydration was performed by exposing relyophilized powder to vapor diffusion in a sealed chamber until the water content reached about 35% by weight, which roughly corresponds to one full hydration layer[34,35] and is a typical threshold at which most globular proteins are fully hydrated,[34,35] so that their internal dynamics is similar to those in solution state.[36]

Deuteron Solid-State NMR Spectroscopy. Experiments below 140 K were performed at 11.7 T spectrometer equipped with a static cryogenic helium-cooled probe.[37] The cryogenic probe had a temperature sensor in immediate proximity to the sample area, and its reading was taken as the sample temperature. Zeeman relaxation time T_1 measurements were performed by the inversion recovery (above 110 K) or saturation recovery (below 110 K) sequences using a multiple echo acquisition (QCPMG, quadrupole Carr−Purcell−Meiboom−Gill) detection scheme for signal-to-noise enhancement.[38] Ten to fifteen QCPMG echoes were collected with 50 μs period corresponding to QCPMG spikelets (sidebands) spaced at 20 kHz intervals for samples with labels on L61 and L75. Data for L69 were taken from a previous work[28] and used echo time of 100 μs. The durations of 90° pulses were between 2.9 and 2.5 μs. Six relaxation delays were typically used above 110 K and four to five below 110 K. The number of scans varied greatly from 64 to 28k, depending on signal-to-noise ratio and the relaxation time constraints at each temperature.

Data were processed with the line broadening of 1 kHz and a baseline correction. T_1 relaxation times were obtained by fitting the signal intensities at selected frequencies of spectra as a function of relaxation delays to the monoexponential inversion recovery or saturation recovery functions. The signal intensities for spikelets with opposite signs of frequencies were averaged. The errors in the relaxation times were estimated by the asymptotic covariance matrix method. The uncertainties in intensities in Figures 6 and 7 were taken from the noise level and may be somewhat underestimated due to slight baseline distortions from residual probe ringing. This issue is most apparent close to the intermediate regime. All processing has been done using Matlab-based scripts.

Numerical Computations. Calculations of the magnetization buildup curves according to eqs 1−3, introduced in the Results and Discussion section, can be performed based on standard expressions for the longitudinal relaxation rates due to the three-site hop mechanism[39] and the expression for the signal intensity.[40,41] However, the final integration in eq 1 has to be performed numerically. Therefore, we can start using the numerical approach, which can also explicitly include the multiple echo acquisition scheme (QCPMG), at an earlier stage of the calculations.

Analytical formulas relating the rate constants to the relaxation times and intensity loss cannot be applied for the QCPMG detection scheme, because each point in the QCPMG spectrum has a different mix of frequencies compared to the regular quadrupolar echo detected powder pattern.[38,42,43] Instead, we used the EXPRESS program to generate magnetization buildup curves for individual conformers and then obtained overall magnetization by numerical integration of eq 1.

EXPRESS[44] is a freely available program for simulation of NMR experiments. It is capable of calculating the frequency-dependent relaxation rates based on experimental parameters as well as parameters characterizing the spin system and geometry. In our case, the most important input parameters are the type of the detection scheme, the echo interpulse delay, quadrupolar coupling constant (either 160 or 175 kHz), three-site hop rates, and the geometry around the methyl carbon (either 68.85° or 70.5° for the angle between the C−D bond and the methyl axis) . The EXPRESS program uses time domain simulations of the NMR experiment and, therefore, naturally includes the dependence of the overall intensity on the interplay of C_q, the interpulse delay of the echo train, as well as the orientation dependence of transverse relaxation.[40,41] We emphasize that the use of EXPRESS instead of the analytical formulas (appropriate for quadrupolar echo detection scheme[5]) does not change the results qualitatively.

RESULTS AND DISCUSSION

Abrupt Rise in T_1 and Spectral Changes Occur in the Same Temperature Range. Figure 1 summarizes the main experimental result of this paper. The apparent relaxation times T_1, defined by single-exponential fit to the data (see Materials and Methods section), experience a jump toward significantly larger values at temperatures below about 90 K. We have previously reported this phenomenon for the methyl groups of L69, and here we observe a similar trend for the methyl groups of L61 and L75. The jump in T_1 values between the temperatures of about 100 and 85 K is by a factor of at least

dx.doi.org/10.1021/jp4021596 | J. Phys. Chem. B 2013, 117, 6129−6137

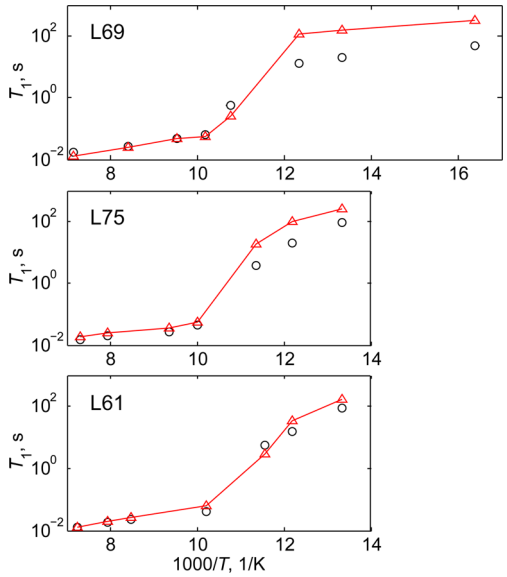

Figure 1. T_1 vs 1000/T. Experimental (black circles) and simulated (red triangles) longitudinal relaxation times in the 140−60 K temperature range. The lines are shown to guide the eye. Experimental error bars are within the size of the symbols. Most of the experimental data for L69 were taken from a previous work.[28]

80. This is a much faster change compared to what might have been predicted if only temperatures higher than 100 K or lower than 85 K were observed.

In the same temperature range at which the jump in T_1 occurs, the overall spectral appearance changes from motionally narrowed Pake-like patterns to a wider transitional shape. At low temperatures the shapes correspond to full-width Pake patterns, with the widths increased by a factor of about 3 from the motionally narrowed spectra. The spectral appearance for different motional regimes is demonstrated in Figure 2. The experiments were conducted using the multiple echo acquisition scheme (QCPMG),[38] which was important for signal enhancement in these protein samples with low sensitivity. We emphasize that this detection scheme serves purely as a signal enhancement tool and is not essential to the phenomenon described in this work. QCPMG breaks the powder pattern into a series of peaks (spikelets), and the distance between these spikelets is governed by the interpulse delay in the echo train. The spectra for L69 were collected with 10 kHz distance between the spikelets, while the new data for L61 and L75 were collected with 20 kHz distances for further signal enhancement.

The relaxation times in the 140−100 K range (Figure 1) correspond to the spikelets with the highest intensity in this spectral range, which are at ±10 kHz frequencies for L69 and at ±20 kHz for L61 and L75. For temperatures lower than 90 K, the relaxation times at ±60 kHz frequencies are shown. All relaxation times were obtained with monoexponential fits. The spikelet at 0 kHz was never chosen, even for the temperature region at which it has the highest intensity because the magnetization recovery curve is very far from single-exponential for the central spikelets around the apparent transition temperature. The nonexponentiality issue will be discussed in detail below. At the lowest temperature point for each residue, we no longer observe any differences in the relaxation times measured for different spikelets. The switch from the −20 to 20 kHz range at higher temperatures to ±60 kHz frequencies at

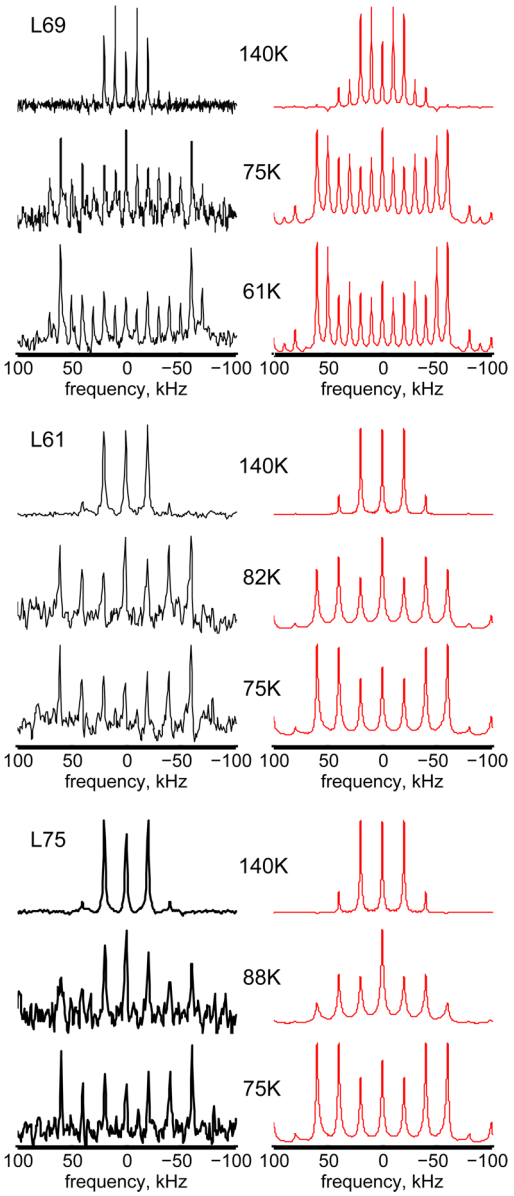

Figure 2. Experimental (black) and simulated (red) QCPMG spectra for methyl groups in three leucine residues illustrating three types of patterns: motionally narrowed (top of each panel), intermediate (middle), and full width (bottom).

lower temperatures cannot in itself be responsible for the apparent transition. The reason for this is that, for a single three-site hop motional process, the relaxation anisotropy cannot exceed the factor of 1.3.[39,43] We also note that, after additional measurements and analysis, which showed strong nonexponentiality, we had to exclude the 0 kHz point at 84 K for L69, which was shown in the original data (Vugmeyster et al.,[28] Figure 2). At this temperature, the frequencies at ±60 kHz were still not discernible from the noise background. An additional data point at 81 K revealed the presence of ±60 kHz spikelet, and the T_1 value corresponding to these frequencies is included in Figure 1.

Theoretical Description of the Effect. In the search for a mechanism that explains the observed jump in the relaxation times, we noted a strong connection between the transition temperature and the spectral changes. This is suggestive of the fact that we are looking at multiple conformers undergoing

dx.doi.org/10.1021/jp4021596 | J. Phys. Chem. B 2013, 117, 6129−6137

changes into the intermediate motional regime (with respect to the quadrupolar coupling constant) at different temperatures. The presence of multiple conformers is in line with our earlier model developed in order to describe the relaxation data in the 300−140 K temperature range.[30]

In this model, the conformers are distinguished by their unique values of activation energy barrier for three-site hop E_a. We do not make any assumptions or connections to the potential energy of the conformers. For a continuous distribution of conformers, the overall observed magnetization $M(t)$ is defined by

$$\int m(E_a, t)\, dE_a = M(t) \tag{1}$$

in which $m(E_a,t)$ is the magnetization density. The distribution of the activation energies is assumed to have a Gaussian form $f(E_a) = [1/(2\pi\sigma^2)]\exp[-(E_a - \langle E_a\rangle)^2/(2\sigma^2)]$. It was chosen as the simplest form that is consistent with the experimental data. The longitudinal relaxation rate depends on the activation energy through the three-site hop rate constant k. Assuming the Arrhenius law for each conformer, $k(E_a,T) = k_0 e^{-E_a/T}$. Arrhenius law has been shown to be valid for methyl groups in several amino acid systems with limited conformational heterogeneity.[45] We also assumed that the value of k_0 is the same for all conformers. Lifting this limitation did not improve the quality of the fit.

In the intermediate regime, at which the three-site jump constant $k(E_a,t)$ becomes comparable to C_q, the signal is characterized by a drastic loss of intensity[40,41] that has to be taken into account when calculating relaxation times and the spectra of multiple conformers at low temperatures. This effect has been considered in detail by Wittebort et al.[40] and Beshah et al.[41] for the quadrupolar echo detection scheme, as well as by Larsen et al.[42] specifically for the QCPMG detection scheme. The origin of the intensity loss lies in the orientational dependence of the transverse relaxation times. For certain orientations of crystallites in a powder sample, the transverse relaxation time (T_2) becomes comparable to the echo interpulse delay, and for these orientations the signal is not refocused by the pulse train. Thus, the intensity is a function of frequency of the powder pattern, as well as the interpulse delay. The latter is kept constant in our experiment.

Wittebort et al.[40] and Beshah et al.[41] report the intensity loss as a function of three-site hop rate. However, because our model describes the conformation ensemble in terms of the distribution of activation energies, it is instructive to look at the intensity loss as a function of E_a and temperature. The intensity loss function thus becomes $I = I(E_a,T,\omega)$.

In Figure 3 we show how the intensity varies as a function of E_a for several fixed temperatures. The details of the simulations are described in the Materials and Methods section. The intensity function for ±10 kHz frequency shows a dramatic drop for the intermediate values of the activation energies, with the position of the minimum shifting with temperature. In addition to the T_2 effect, the intensity at a particular frequency is also affected by the overall width of the spectrum. The motional narrowing of the spectrum, occurring for high jump rates ($k \gg C_q$), naturally leads to higher intensities for the frequencies inside the narrowed spectral range when compared to the full-size spectrum for lower jump rates. This is why at high values of E_a (corresponding to small value of k) the intensity function levels out to about 2/3 of the maximum. The spectral changes are also the reason why the intensity function

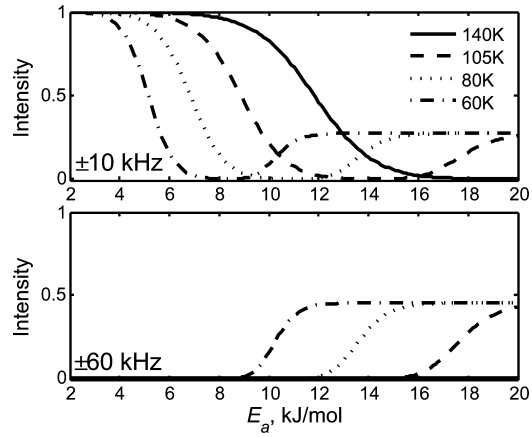

Figure 3. Simulated intensities $I(E_a,\omega)$ for ±10 and ±60 kHz spikelets of the QCPMG spectrum as a function of activation energy E_a at four temperatures. The pre-exponential factor is $k_0 = 5.3 \times 10^{11}$ s^{-1}, the interpulse echo delay is 100 μs, and the Larmor frequency is 76.78 MHz (corresponding to 11.7 T). The scale is chosen in such a way that $I(E_a,\omega) = 1$ for $E_a = 0$ at $\omega = \pm 10$ kHz at each temperature.

looks different for ±60 kHz spikelets, as at ±60 kHz there is negligible intensity for the motionally narrowed spectra. The position of the intensity loss for the ±60 kHz spikelets shifts with temperature analogous to the behavior at ±10 kHz. For 140 K, the rise of intensity at high values of E_a is cut by the upper boundary of the E_a-axis in Figure 3.

The expression for $m(E_a,t)$ at a specific temperature can be split into three separate contributions

$$m(E_a, t, \omega) = f(E_a) I(E_a, \omega) R(E_a, t, \omega) \tag{2}$$

in which $R(E_a,t,\omega)$ characterizes the time dependence of magnetization in a chosen experimental scheme:

$$R(E_a, t, \omega) = \begin{cases} 1 - \exp(-t/T_1(E_a, \omega)) & \text{saturation recovery} \\ 1 - 2\exp(-t/T_1(E_a, \omega)) & \text{inversion recovery} \end{cases} \tag{3}$$

$T_1(E_a,\omega)$ is a longitudinal relaxation time of the conformer with activation energy E_a at a chosen value of frequency. The frequency dependence of $T_1(E_a,\omega)$ in an individual conformer reflects the relaxation anisotropy due to three-site hop mechanism.

Equation 1 shows that the contribution of each conformer into the overall magnetization is weighted by $\tilde{f}(E_a,\omega) = f(E_a) I(E_a,\omega)$, which can be quite different from the Gaussian distribution $f(E_a)$. Figure 4 illustrates how the effect of the intensity loss in the intermediate regime skews the real Gaussian form of the distribution function. The effective distribution is shown for ±10 kHz spikelet of the QCPMG scheme in the left column and for ±60 kHz spikelet in the right column. The parameters of the distribution are chosen as $\langle E_a\rangle$ = 12 kJ/mol, and σ = 1.5 kJ/mol, which are typical values that we obtained for the 298−140 K range for the same methyl groups in HP36 protein. Twelve kJ/mol also falls in the center of the range of typical activation energy barriers measured for other proteins.[6] It is clear that the fraction of the signal due to conformers in the intermediate regime is severely reduced, which leads to the apparent relaxation times being governed primarily by the conformers in either the fast regime (higher temperatures) or slow regime (low temperatures). When the

dx.doi.org/10.1021/jp4021596 | J. Phys. Chem. B 2013, 117, 6129−6137

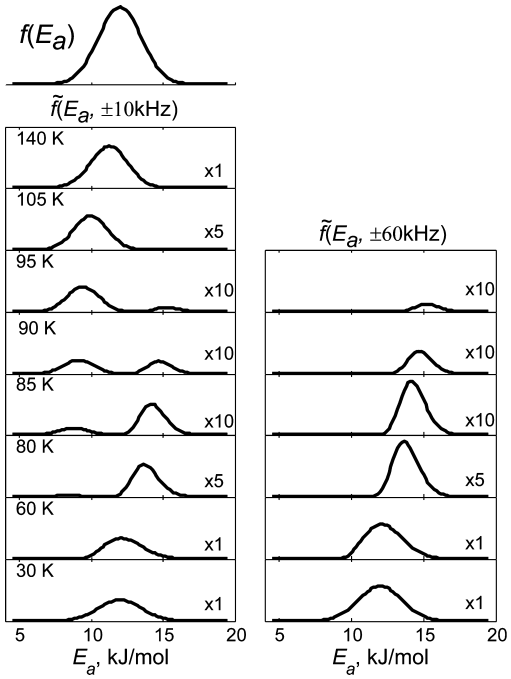

Figure 4. Effective probability distribution $\tilde{f}(E_a,\omega) = f(E_a)I(E_a,\omega)$ for ±10 kHz (left column) and ±60 kHz (right column) for several temperatures. Relative scaling factors are shown in the right bottom corner.

conformers in the center of the distribution are in the intermediate regime, the effective distribution becomes bimodal for the ±10kHz frequency, giving rise to especially strong nonexponentiality. For the ±60 kHz spikelets the situation is somewhat different, as at high temperatures there is negligible signal intensity at these frequencies. As the temperature is lowered, more and more conformers undergo a switch toward a full-width powder pattern and, thus, the contribution at the ±60 kHz frequencies increases. Therefore, the effective distribution for the ±60 kHz frequencies is never bimodal.

The existence of the activation energy distribution is reflected in the nonexponentiality of the magnetization recovery curves. In order to describe the temperature dependence of the magnetization recovery curves, it is desirable to select several parameters that characterize the curves and follow the temperature dependence of these parameters. For a unimodal distribution of relaxation rates, a common choice is a phenomenological parametrization of the magnetization recovery curve via the stretched exponential function.[46−48] However, in more general cases the stretched exponential function is not necessarily an adequate representation of the recovery curve. An example of this is the bimodal distribution depicted in Figure 4 for 90 K at 10 kHz. Therefore, we chose to characterize the curves by three parameters which do not directly contain the information about the shape, but rather emphasize different subsets of the distribution. Each of the three parameters coincides with the conventional definition of T_1 for a monoexponential recovery. The first parameter given by $\langle 1/T_1(E_a)\rangle^{-1}$ emphasizes the contribution of conformers with fast relaxation rates and is proportional to the initial slope of the recovery curve:

$$\langle 1/T_1(E_a)\rangle = -\frac{1}{M(0) - M(\infty)}\frac{dM(t)}{dt}\bigg|_{t=0} \quad (4)$$

To simplify the notation, we do not show the explicit dependence on the frequency of the powder pattern ω. The second parameter

$$\langle T_1(E_a)\rangle = \frac{\int_0^\infty (M(t) - M(\infty))\,dt}{M(0) - M(\infty)} \quad (5)$$

depends mainly on the long times tail of the recovery curve and therefore emphasizes the contribution from the slow conformers. In eqs 4 and 5 we denote $\langle X(E_a)\rangle$ as the following ensemble average

$$\langle X(E_a)\rangle = \frac{\int X(E_a)\tilde{f}(E_a,\omega)\,dE_a}{\int \tilde{f}(E_a,\omega)\,dE_a} \quad (6)$$

The interrelation between $\langle 1/T_1(E_a)\rangle^{-1}$ and $\langle T_1(E_a)\rangle$ has been discussed earlier, for example, by Geil and Hinze.[49]

Finally, we introduce the third parameter T'_1 which is influenced in a more uniform way by both sides of the distribution and is defined by

$$M(\infty) - M(T'_1) = (M(\infty) - M(0))/e \quad (7)$$

We will now demonstrate that the existence of the distribution leads to a sharp rise in all three of these parameters, T'_1, $\langle 1/T_1(E_a)\rangle^{-1}$, and $\langle T_1(E_a)\rangle$.

We first look in detail at the temperature dependence of T'_1, calculated as described in the Materials and Methods section. Figure 5A shows simulated values of T'_1 for $\langle E_a\rangle$ = 12 kJ/mol

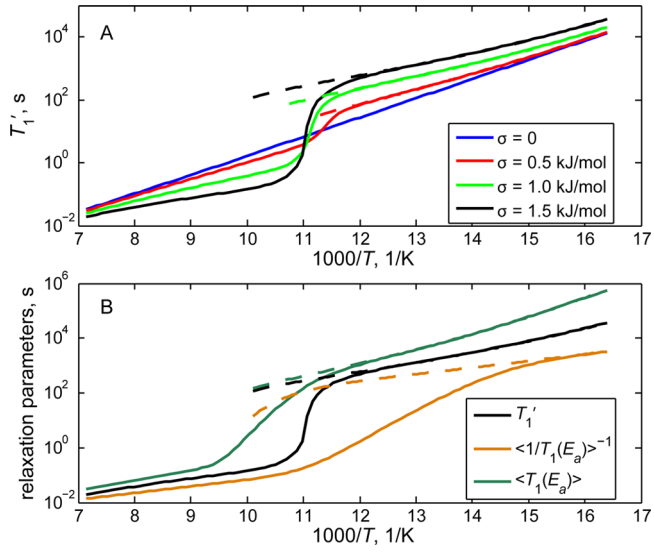

Figure 5. (A) Simulated characteristic relaxation times T'_1 in QCPMG saturation recovery experiment as function of $1000/T$ for the model with a Gaussian distribution of activation energies for different values of the width σ. (B) Simulated values of $\langle 1/T_1(E_a)\rangle^{-1}$, $\langle T_1(E_a)\rangle$, and T'_1 for σ = 1.5 kJ/mol. The central value of $\langle E_a\rangle$ = 12 kJ/mol and the Larmor frequency is 76.78 MHz (corresponding to 11.7 T). Solid lines correspond to ±10 kHz spikelets, dashed lines correspond to ±60 kHz spikelets.

and different values of σ. As expected, when the width of the distribution is zero, T'_1 follows the Arrhenius law. When σ is gradually increased, the plots become sigmoidal-like and the steepness of the curve in the transition region increases. The temperature of the transition region is relatively unchanged with σ. Away from the transition region, the slope of the T'_1

dx.doi.org/10.1021/jp4021596 | J. Phys. Chem. B 2013, 117, 6129−6137

curve is smaller for larger values of σ. As can be seen from Figure 4, for temperatures higher than those in the transition region, the position of the maximum of the effective activation energy distribution $\tilde{f}(E_a,\omega)$ is gradually shifting to the lower values of E_a when the temperature is lowered. Thus, typical three-site hop rate constants are shifting to the higher values and typical relaxation times are, in turn, shifted to the lower values. This reduces the slope of the T'_1 curve. Just after the transition region, the maximum of $\tilde{f}(E_a,\omega)$ is achieved at much larger values of E_a, but the direction of its change resumes the previous trend, once again manifesting itself in the smaller slope of the T'_1 curve.

The transition is also apparent for both $\langle 1/T_1(E_a)\rangle^{-1}$ and $\langle T_1(E_a)\rangle$, as demonstrated in Figure 5B for the case of σ = 1.5 kJ/mol. The temperature of the apparent transition is somewhat different depending at which parameter one chooses to look. As expected, the actual values T'_1 are in between the values calculated for $\langle 1/T_1(E_a)\rangle^{-1}$ and $\langle T_1(E_a)\rangle$. It is important to emphasize that in this work we are considering the situation in which there is no conformational exchange between the substates on the time scale of longitudinal relaxation times. Thus, in our case the apparent transition is not due to crossover from exponential to nonexponential decay. This "glassy" crossover is a well-studied phenomenon and was described in detail for example by Geil and Hinze[49] and Schnauss et al.[50]

We note that the model does not connect the values of the activation energies to the structural origin of the conformational substates. The differences in the activation energies, in principle, can stem either from slow motions of the methyl axis, or, alternatively, from larger scale motions in the hydrophobic core that affect the local environment around the methyl group of interest.

Application of the Model to Relaxation Data in HP36 in the 140−70 K Range. Quantitative experimental measurements of all three parameters $\langle 1/T_1(E_a)\rangle^{-1}$, $\langle T_1(E_a)\rangle$, and T'_1 introduced in the theory section require a reliable knowledge of the value of $M(\infty)$. For low-sensitivity samples and large relaxation times this becomes unfeasible. We are only capable of sampling the initial portion of the recovery curve. Away from the transition region, these initial recovery curves are fitted well with the single-exponential function (Figure 6). Out of the three parameters defined in the theory section, this way of measurement corresponds most closely to the $\langle 1/T_1(E_a)\rangle^{-1}$.[47] The data in Figure 1 conveys the main experimental effect, namely the jump in the relaxation times T_1 of orders of magnitude. In order to minimize any distortions in the fitting procedure due to nonexponentiality and the uncertainty in the value of $M(\infty)$, the simulated relaxation times used for comparison with the experiment are obtained by selecting points corresponding to the same time delays as were used in the experiment and fitting them with the single-exponential function.

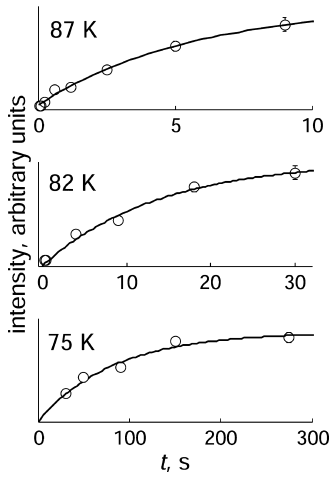

Figure 6. Experimental saturation recovery curves (circles) and monoexponential fits (lines) for L61 residue for three intermediate and low temperatures.

In the simulations we assumed that the parameters of the activation energy distribution are temperature independent and used the values obtained earlier for the 300−140 K temperature range.[30] This temperature range is far from the transition region and the observed relaxation times were relatively short. Therefore, we were able to reliably define long time nonexponential tails of $M(t)$, which are critical in determining the parameters of $f(E_a)$. The parameters of the distribution are listed in section SI2 in the Supporting Information. We also note that because of the 1:1 ratio in the labeling pattern of CD_3 groups of leucine side chain, the overall results represent an average between the two methyl groups.

Figure 1 demonstrates a reasonable agreement between the modeled and experimental values of T_1, although it misses the exact values of T_1 at low temperatures. The jump in T_1 is predicted in the correct temperature range. It is important that the modeled values reproduce experimental "pretransition" T_1 values in the 140−110 K range adequately. The data in this work were obtained at 11.7 T, as opposed to the field of 17.6 T for the high-temperature range used in the determination of the distribution parameters. As can be seen from the theoretical calculations in Figure 5A, the existence of the distribution significantly affects relaxation times even for temperatures well outside the transition region. In addition, as the relaxation times of individual conformers are field-dependent, the influence of the width of distribution on T_1 depends on the field strength as well. Thus, the fact that the data are fitted well with the same distribution parameters over a wide temperature range at two different field strengths validates our model.

We also note that within our model the linear term in the dependence of activation energy on temperature cannot be detected, as it would be disguised as a different fitted value of k_0. However, large nonlinear deviations should be apparent from comparing theory and experiment. The fact that the same distribution parameters work well in the wide temperature range between 300 and 90 K suggests that the hydrophobic core packing (environment) is roughly temperature independent.

At about 90−80 K temperature range the bimodal effective distribution of the activation energies (Figure 4) leads to especially strong nonexponentiality for the −20 to 20 kHz range. Thus, we cannot apply the single-exponential approximation and define the values of T_1. At these temperatures, the spikelets at ±60 kHz, for which the single-exponential approximation would be reasonable, are still not discernible in the spectra. Thus, Figure 1 has a gap in this range. Nevertheless, we can still demonstrate an agreement between theory and experiment in this temperature region by comparing simulated and experimental magnetization recovery curves, as shown in Figure 7.

One of the possible reasons for the deviations between experimental and simulated data at low temperatures is the fact that the model does not take into account the effect of

dx.doi.org/10.1021/jp4021596 | J. Phys. Chem. B 2013, 117, 6129−6137

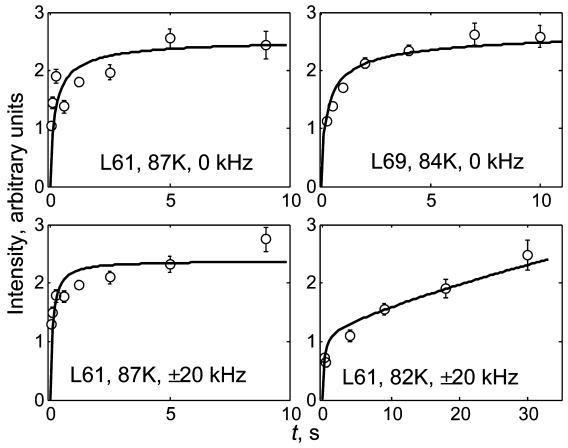

Figure 7. Experimental (circles) and simulated (lines) magnetization buildup curves for L61 and L69 in the −20 to +20 kHz range at intermediate temperatures. The absolute intensities of the simulated curves are scaled to the experimental data.

deuteron tunneling. Deuteron tunneling is known to be an important relaxation mechanism at cryogenic temperatures[51−54] and is likely to be a dominant mechanism below about 30 K.[51] In section SI3 in the Supporting Information we show that the inclusion of the tunneling effect improves the agreement between the simulated and experimental T_1 values at low temperatures.

The fact that the relaxation behavior for all three residues is similar, although not identical, suggests a possibility that the conformational ensemble that defines the distribution of the activation energies is governed by common fluctuations in the hydrophobic core.

The model also correctly reproduces the main features in the temperature dependence of the experimental spectra (Figure 2), namely the change from the motionally narrowed pattern to the transitional spectra, and then to the full-width pattern. We note that the experimental spectra represent the spectra collected with the longest delay in the relaxation experiment. The simulated spectra were obtained using the same relaxation delays.

The simulated spectra used the value of C_q = 160 kHz, which was chosen based on the quadrupolar echo spectra of all leucine residues in the fast motional regime, which had the effective quadrupolar splitting of 53.3 kHz.[27,55] However, at lower temperatures there are slight discrepancies between simulated and experimental spectra, which are more consistent with a somewhat larger value of C_q = 175 kHz. The differences in the two values of the quadrupolar constant are reconciled if we allow a nontetrahedral geometry of the methyl carbon with the angle of 68.85° between the methyl axis and the C−D bond, compared to 70.5° for the tetrahedral geometry. This issue is explored in more detail in section SI4 in the Supporting Information.

There has been a growing interest in protein dynamics at low temperatures[16,56−59] in regard to opportunities and challenges that it may pose to low-temperature structural studies using magic angle spinning and dynamic nuclear polarization.[58] The line widths of individual resonances often increase or split into multiple peaks in these experiments at low temperatures.[57,59] Our work can be useful in this respect by offering a unified description of the dynamics of methyl groups from physiological conditions down to cryogenic temperatures and providing insights on the mechanisms of the line-broadening effects.

Comparison with Neutron Scattering Studies. As discussed in the Introduction, neutron scattering measurements showed an inflection in the mean atomic displacement curve as a function of temperature for a number of proteins. The inflection occurs in a similar temperature range between 150 and 100 K. Most current works suggest that the inflection is caused by the fact that the rate constants for methyl hops of individual methyl groups are entering the resolution window of the spectrometer at somewhat different temperatures.[31−33] Of particular interest are the recent works by Wood et al.,[31] which combine neutron scattering experiments with molecular dynamic simulations and NMR results, the work of Roh et al. on lysozyme protein,[32] and the work of Schiro et al.[33] on homomeric polypeptides. All of the neutron scattering studies did not provide site-specific resolution. They often used one type of amino acids, for example, only valine, leucine, or isoleucine residues, but not individual amino acids. It has been implicitly assumed that the differences in methyl three-site hop rates required to explain the observed phenomenon correspond to the variations among different sites.

One of the models suggested for this effect has also included a Gaussian distribution of activation energies for methyl hops.[33] The fitted values for the distribution for myoglobin protein yielded[33] $\langle E_a \rangle$ of 16 kJ/mol and σ of 6 kJ/mol, and $\langle E_a \rangle$ of 17 kJ/mol and σ of 6 kJ/mol for lysozyme.[32] As the samples employed in these studies did not have site-specific labels, it is not possible to distinguish which part of this distribution is due to the variations between the residues as opposed to the variations due to conformational heterogeneity of one specific residue. The width of 6 kJ/mol, as opposed to our typical value on the order of 1.4 kJ/mol, indicates, unsurprisingly, that the width observed through the neutron scattering is primarily due to inter-residue differences. Nevertheless, from our residue-specific results, it follows that the conformational heterogeneity can also be a contributing factor into the origin of low-temperature neutron scattering inflection.

■ CONCLUSION

We have shown that the apparent transition in deuteron NMR longitudinal relaxation times of methyl groups around 90 K can be explained by conformational heterogeneity present in the hydrophobic core. A model based on the existence of a distribution of conformers distinguished only by different activation barriers for three-site methyl hops, combined with the fact that the conformers undergo a switch from the fast to intermediate motional regime at different temperatures, predicts the jump in the T_1 relaxation times. The parameters of the model are consistent throughout a very wide temperature range between 300 and 70 K as well as between two different magnetic field strengths, which provides an important validation of the model.

■ ASSOCIATED CONTENT

Supporting Information

SI1: Ribbon diagram of HP36 protein showing the position of L61, L69, and L75 side chains. SI2: Parameters of the distribution of the activation energies. SI3: Effect of deuteron tunneling. SI4: Detailed analysis of low-temperature spectra. This material is available free of charge via the Internet at http://pubs.acs.org.

dx.doi.org/10.1021/jp4021596 | J. Phys. Chem. B 2013, 117, 6129−6137

AUTHOR INFORMATION

Corresponding Author

*E-mail: lvugmeyster@uaa.alaska.edu. Tel.: (907)786-4709. Fax: 907-786-4607.

Notes

The authors declare no competing financial interest.

ACKNOWLEDGMENTS

This research was funded by National Science Foundation Grants MCB-1122154 to L.V. and D.O. as well as by the Innovate Award of the University of Alaska Anchorage. Experiments were performed using EMSL, a national scientific user facility sponsored by the Department of Energy's Office of Biological and Environmental Research located at Pacific Northwest National Laboratory.

REFERENCES

(1) Igumenova, T. I.; Frederick, K. K.; Wand, A. J. Characterization of the Fast Dynamics of Protein Amino Acid Side Chains Using NMR Relaxation in Solution. *Chem. Rev.* **2006**, *106*, 1672−1699.

(2) Krushelnitsky, A.; Reichert, D. Solid-State Nmr and Protein Dynamics. *Prog. Nucl. Magn. Reson. Spectrosc.* **2005**, *47*, 1−25.

(3) Lee, A. L.; Wand, A. J. Microscopic Origins of Entropy, Heat Capacity and the Glass Transition in Proteins. *Nature* **2001**, *411*, 501−504.

(4) Mittermaier, A. K.; Kay, L. E. Observing Biological Dynamics at Atomic Resolution Using NMR. *Trends Biochem. Sci.* **2009**, *34*, 601−611.

(5) Vold, R. L.; Vold, R. R. Deuterium Relaxation in Molecular Solids. In *Advances in Magnetic and Optical Resonance*; Warren, W., Ed.; Academic Press: San Diego, CA, 1991; pp 85−171.

(6) Xue, Y.; Pavlova, M. S.; Ryabov, Y. E.; Reif, B.; Skrynnikov, N. R. Methyl Rotation Barriers in Proteins from H-2 Relaxation Data. Implications for Protein Structure. *J. Am. Chem. Soc.* **2007**, *129*, 6827−6838.

(7) Meints, G. A.; Miller, P. A.; Pederson, K.; Shajani, Z.; Drobny, G. Solid-State Nuclear Magnetic Resonance Spectroscopy Studies of Furanose Ring Dynamics in the DNA Hhal Binding Site. *J. Am. Chem. Soc.* **2008**, *130*, 7305−7314.

(8) Olsen, G. L.; Bardaro, M. F.; Echodu, D. C.; Drobny, G. P.; Varani, G. Hydration Dependent Dynamics in RNA. *J. Biomol. NMR* **2009**, *45*, 133−142.

(9) McDermott, A.; Polenova, T. Solid State Nmr: New Tools for Insight into Enzyme Function. *Curr. Opin. Struct. Biol.* **2007**, *17*, 617−622.

(10) Fu, Y. N.; Kasinath, V.; Moorman, V. R.; Nucci, N. V.; Hilser, V. J.; Wand, A. J. Coupled Motion in Proteins Revealed by Pressure Perturbation. *J. Am. Chem. Soc.* **2012**, *134*, 8543−8550.

(11) Agarwal, V.; Xue, Y.; Reif, B.; Skrynnikov, N. R. Protein Side-Chain Dynamics as Observed by Solution- and Solid-State Nmr Spectroscopy: A Similarity Revealed. *J. Am. Chem. Soc.* **2008**, *130*, 16611−16621.

(12) Hansen, D. F.; Neudecker, P.; Vallurupalli, P.; Mulder, F. A. A.; Kay, L. E. Determination of Leu Side-Chain Conformations in Excited Protein States by NMR Relaxation Dispersion. *J. Am. Chem. Soc. 132*, 42-47.

(13) Mittermaier, A.; Kay, L. E. The Response of Internal Dynamics to Hydrophobic Core Mutations in the SH3 Domain from the Fyn Tyrosine Kinase. *Protein Sci.* **2004**, *13*, 1088−1099.

(14) Millet, O.; Mittermaier, A.; Baker, D.; Kay, L. E. The Effects of Mutations on Motions of Side-Chains in Protein L Studied by H-2 NMR Dynamics and Scalar Couplings. *J. Mol. Biol.* **2003**, *329*, 551−563.

(15) McKnight, C. J.; Doering, D. S.; Matsudaira, P. T.; Kim, P. S. A Thermostable 35-Residue Subdomain within Villin Headpiece. *J. Mol. Biol.* **1996**, *260*, 126−134.

(16) Hu, K. N.; Havlin, R. H.; Yau, W. M.; Tycko, R. Quantitative Determination of Site-Specific Conformational Distributions in an Unfolded Protein by Solid-State Nuclear Magnetic Resonance. *J. Mol. Biol.* **2009**, *392*, 1055−1073.

(17) Havlin, R. H.; Tycko, R. Probing Site-Specific Conformational Distributions in Protein Folding with Solid-State Nmr. *Proc. Natl. Acad. Sci. U.S.A.* **2005**, *102*, 3284−3289.

(18) Reiner, A.; Henklein, P.; Kiefhaber, T. An Unlocking/Relocking Barrier in Conformational Fluctuations of Villin Headpiece Subdomain. *Proc. Natl. Acad. Sci. U.S.A.* **2010**, *107*, 4955−4960.

(19) Kubelka, J.; Chiu, T. K.; Davies, D. R.; Eaton, W. A.; Hofrichter, J. Sub-Microsecond Protein Folding. *J. Mol. Biol.* **2006**, *359*, 546−553.

(20) Xiao, S. F.; Bi, Y.; Shan, B.; Raleigh, D. P. Analysis of Core Packing in a Cooperatively Folded Miniature Protein: The Ultrafast Folding Villin Headpiece Helical Subdomain. *Biochemistry* **2009**, *48*, 4607−4616.

(21) Vugmeyster, L.; Trott, O.; McKnight, C. J.; Raleigh, D. P.; Palmer, A. G. Temperature-Dependent Dynamics of the Villin Headpiece Helical Subdomain, an Unusually Small Thermostable Protein. *J. Mol. Biol.* **2002**, *320*, 841−854.

(22) Wang, M. H.; Tang, Y. F.; Sato, S. S.; Vugmeyster, L.; McKnight, C. J.; Raleigh, D. P. Dynamic NMR Line-Shape Analysis Demonstrates That the Villin Headpiece Subdomain Folds on the Microsecond Time Scale. *J. Am. Chem. Soc.* **2003**, *125*, 6032−6033.

(23) Wickstrom, L.; Bi, Y.; Hornak, V.; Raleigh, D. P.; Simmerling, C. Reconciling the Solution and X-Ray Structures of the Villin Headpiece Helical Subdomain: Molecular Dynamics Simulations and Double Mutant Cycles Reveal a Stabilizing Cation-Pi Interaction. *Biochemistry* **2007**, *46*, 3624−3634.

(24) Massi, F.; Palmer, A. G. Temperature Dependence of Nmr Order Parameters and Protein Dynamics. *J. Am. Chem. Soc.* **2003**, *125*, 11158−11159.

(25) Chiu, T. K.; Kubelka, J.; Herbst-Irmer, R.; Eaton, W. A.; Hofrichter, J.; Davies, D. R. High-Resolution X-Ray Crystal Structures of the Villin Headpiece Subdomain, an Ultrafast Folding Protein. *Proc. Natl. Acad. Sci. U.S.A.* **2005**, *102*, 7517−7522.

(26) McKnight, C. J.; Matsudaira, P. T.; Kim, P. S. Nmr Structure of the 35-Residue Villin Headpiece Subdomain. *Nat. Struct. Biol.* **1997**, *4*, 180−184.

(27) Vugmeyster, L.; Ostrovsky, D.; Ford, J. J.; D., B. S.; Lipton, A. S.; Hoatson, G. L.; Vold, R. L. Probing the Dynamics of a Protein Hydrophobic Core by Deuteron Solid-State Nuclear Magnetic Resonance Spectroscopy. *J. Am. Chem. Soc.* **2009**, *131*, 13651−13658.

(28) Vugmeyster, L.; Ostrovsky, D.; Ford, J. J.; Lipton, A. S. Freezing of Dynamics of a Methyl Group in a Protein Hydrophobic Core at Cryogenic Temperatures by Deuteron NMR Spectroscopy. *J. Am. Chem. Soc.* **2010**, *132*, 4038−4039.

(29) Abragam, A. *Principles of Nuclear Magnetism*; Clarendon Press: Oxford, UK, 1961.

(30) Vugmeyster, L.; Ostrovsky, D.; Penland, K.; Hoatson, G. L.; Vold, R. L. Glassy Dynamics of Protein Methyl Groups Revealed by Deuteron NMR. *J. Phys. Chem. B* **2013**, *117*, 1051−1061.

(31) Wood, K.; Tobias, D. J.; Kessler, B.; Gabel, F.; Oesterhelt, D.; Mulder, F. A. A.; Zaccai, G.; Weik, M. The Low-Temperature Inflection Observed in Neutron Scattering Measurements of Proteins Is Due to Methyl Rotation: Direct Evidence Using Isotope Labeling and Molecular Dynamics Simulations. *J. Am. Chem. Soc.* **2010**, *132*, 4990−4991.

(32) Roh, J. H.; Novikov, V. N.; Gregory, R. B.; Curtis, J. E.; Chowdhuri, Z.; Sokolov, A. P. Onsets of Anharmonicity in Protein Dynamics. *Phys. Rev. Lett.* **2005**, *95*, 038101−1−038101−4.

(33) Schiro, G.; Caronna, C.; Natali, F.; Cupane, A. Direct Evidence of the Amino Acid Side Chain and Backbone Contributions to Protein Anharmonicity. *J. Am. Chem. Soc.* **2010**, *132*, 1371−1376.

(34) Rupley, J. A.; Gratton, E.; Careri, G. Water and Globular-Proteins. *Trends Biochem. Sci.* **1983**, *8*, 18−22.

(35) Khodadadi, S.; Pawlus, S.; Sokolov, A. P. Influence of Hydration on Protein Dynamics: Combining Dielectric and Neutron Scattering Spectroscopy Data. *J. Phys. Chem. B* **2008**, *112*, 14273−14280.

(36) Krushelnitsky, A.; Zinkevich, T.; Mukhametshina, N.; Tarasova, N.; Gogolev, Y.; Gnezdilov, O.; Fedotov, V.; Belton, P.; Reichert, D. C-13 and N-15 NMR Study of the Hydration Response of T4 Lysozyme and Alpha B-Crystallin Internal Dynamics. *J. Phys. Chem. B* **2009**, *113*, 10022−10034.
(37) Lipton, A. S.; Heck, R. W.; Sears, J. A.; Ellis, P. D. Low Temperature Solid-State NMR Experiments of Half-Integer Quadrupolar Nuclides: Caveats and Data Analysis. *J. Magn. Reson.* **2004**, *168*, 66−74.
(38) Larsen, F. H.; Jakobsen, H. J.; Ellis, P. D.; Nielsen, N. C. High-Field Qcpmg-Mas NMR of Half-Integer Quadrupolar Nuclei with Large Quadrupole Couplings. *Mol. Phys.* **1998**, *95*, 1185−1195.
(39) Torchia, D. A.; Szabo, A. Spin-Lattice Relaxation in Solids. *J. Magn. Reson.* **1982**, *49*, 107−121.
(40) Wittebort, R. J.; Olejniczak, E. T.; Griffin, R. G. Analysis of Deuterium Nuclear-Magnetic-Resonance Line-Shapes in Anisotropic Media. *J. Chem. Phys.* **1987**, *86*, 5411−5420.
(41) Beshah, K.; Olejniczak, E. T.; Griffin, R. G. Deuterium NMR-Study of Methyl-Group Dynamics in L-Alanine. *J. Chem. Phys.* **1987**, *86*, 4730−4736.
(42) Larsen, F. H.; Jakobsen, H. J.; Ellis, P. D.; Nielsen, N. C. Molecular Dynamics from H-2 Quadrupolar Carr-Purcell-Meiboom-Gill Solid-State NMR Spectroscopy. *Chem. Phys. Lett.* **1998**, *292*, 467−473.
(43) Vold, R. L.; Hoatson, G. L.; Vugmeyster, L.; Ostrovsky, D.; De Castro, P. J. Solid State Deuteron Relaxation Time Anisotropy Measured with Multiple Echo Acquisition. *Phys. Chem. Chem. Phys.* **2009**, *11*, 7008−7012.
(44) Vold, R. L.; Hoatson, G. L. Effects of Jump Dynamics on Solid State Nuclear Magnetic Resonance Line Shapes and Spin Relaxation Times. *J. Magn. Reson.* **2009**, *198*, 57−72.
(45) Batchelder, L. S.; Niu, C. H.; Torchia, D. A. Methyl Reorientation in Polycrystalline Amino-Acids and Peptides - a H-2 NMR Spin-Lattice Relaxation Study. *J. Am. Chem. Soc.* **1983**, *105*, 2228−2231.
(46) Kohlarausch, R. Theorie Des Elektrischen Rückstandes. *Der Leidner Flasche* **1854**, *91*, 179−213.
(47) Beckmann, P. A.; Schneider, E. Methyl Group Rotation, H-1 Spin-Lattice Relaxation in an Organic Solid, and the Analysis of Nonexponential Relaxation *J. Chem. Phys.* **2012**, *136*.
(48) Sillescu, H. Heterogeneity at the Glass Transition: A Review. *J. NonCryst. Sol.* **1999**, *243*, 81−108.
(49) Geil, B.; Hinze, G. Influence of Data Treatment on the Shape of H-2 NMR T(1) Curves. *Chem. Phys. Lett.* **1993**, *216*, 51−55.
(50) Schnauss, W.; Fujara, F.; Hartmann, K.; Sillescu, H. Nonexponential H-2 Spin-Lattice Relaxation as a Signature of the Glassy State. *Chem. Phys. Lett.* **1990**, *166*, 381−384.
(51) Diezemann, G.; Sillescu, H.; van der Putten, D. Spin-Lattice Relaxation Rates of Tunneling CD3 Groups. *Z. Phys. B: Condens. Matter* **1991**, *83*, 245−257.
(52) Heuer, A. Quantum-Mechanical Behavior of Deuterated Methyl-Groups - the Temperature Dependences of NMR-Spectra and Spin-Lattice Relaxation-Times. *Z. Phys. B* **1992**, *88*, 39−51.
(53) Horsewill, A. J. Quantum Tunnelling Aspects of Methyl Group Rotation Studied by NMR. *Prog. Nucl. Magn. Reson. Spectrosc.* **1999**, *35*, 359−389.
(54) Latanowicz, L. Nmr Relaxation Study of Methyl Groups in Solids from Low to High Temperatures. *Concepts Magn. Reson., Part A* **2005**, *27A*, 38−53.
(55) Vugmeyster, L.; Ostrovsky, D.; Khadjinova, A.; Ellden, J.; Hoatson, G. L.; Vold, R. L. Slow Motions in the Hydrophobic Core of Chicken Villin Headpiece Subdomain and Their Contributions to Configurational Entropy and Heat Capacity from Solid-State Deuteron NMR Measurements. *Biochemistry* **2011**, *50*, 10637−10646.
(56) Siemer, A. B.; Huang, K. Y.; McDermott, A. E. Protein Linewidth and Solvent Dynamics in Frozen Solution NMR. *PLoS One* **2012**, *7*, 1−8.
(57) Linden, A. H.; Franks, W. T.; Akbey, U.; Lange, S.; van Rossum, B. J.; Oschkinat, H. Cryogenic Temperature Effects and Resolution Upon Slow Cooling of Protein Preparations in Solid State NMR. *J. Biomol. NMR* **2011**, *51*, 283−292.
(58) Barnes, A. B.; De Paepe, G.; van der Wel, P. C. A.; Hu, K. N.; Joo, C. G.; Bajaj, V. S.; Mak-Jurkauskas, M. L.; Sirigiri, J. R.; Herzfeld, J.; Temkin, R. J.; Griffin, R. G. High-Field Dynamic Nuclear Polarization for Solid and Solution Biological NMR. *Appl. Magn. Reson.* **2008**, *34*, 237−263.
(59) Bajaj, V. S.; van der Wel, P. C. A.; Griffin, R. G. Observation of a Low-Temperature, Dynamically Driven Structural Transition in a Polypeptide by Solid-State NMR Spectroscopy. *J. Am. Chem. Soc.* **2009**, *131*, 118−128.